Characterization of flow reduction properties in an aneurysm due to a stent

Miki Hirabayashi,[1] Makoto Ohta,[2] Daniel A. Rüfenacht,[2] and Bastien Chopard[1]
[1]*CUI, Department d'Informatique, University of Geneva, 24 rue du General-Dufour, CH-1211 Geneva 4, Switzerland*
[2]*Department of Neuroradiology, Hospital University of Geneva, 24 rue Michelli-du-Crest, CH1211 Geneva 14, Switzerland*
(Received 5 March 2003; published 26 August 2003)

We consider a lattice Boltzmann simulation of blood flow in a vessel deformed by the presence of an aneurysm. Modern clinical treatments involve introducing a stent (a tubular mesh of wires) into the cerebral artery in order to reduce the flow inside the aneurysm and favor its spontaneous reabsorption. A crucial question is to design the stent with suitable porosity so as to produce the most effective flow reduction. We propose a stent positioning factor as a characterizing tool for stent pore design in order to describe the flow reduction effect and reveal the several flow reduction mechanisms using this effect.

DOI: 10.1103/PhysRevE.68.021918 PACS number(s): 87.80.−y, 87.90.+y

Hemodynamics has now become an important field of research for numerical simulations [1] because a better understanding of the behavior of blood flow in various organs is a very challenging issue in medical research. Here we present a numerical study of the hemodynamics of a cerebral artery on which a saccular aneurysm has developed.

To a crude approximation, such a situation is similar to a cavity flow: the aneurysm can be considered as a semicircular or a circular deformation in the vessel membrane, as shown in Fig. 1. As blood flows in the vessel, it produces a circulation inside the cavity. It turns out that the flow inside the aneurysm is detrimental to the thrombus effect, that is, the deposition of blood constituents on the aneurysm wall. The thrombus formation is the natural way for blood to clot at the wall, leading to the reabsorption of the aneurysm. Without this effect, the aneurysm may grow and possibly break, thus causing a hemorrhage that can be lethal.

To prevent this dangerous rupture a modern and minimally invasive treatment of cerebral aneurysms, which involves introducing a stent into the vessel so as to occlude partially the orifice of the cavity, was proposed in 1994 [2,3]. Stents are tubular meshes made of stainless steel or alloys, as shown in Fig. 2. If a suitable stent is chosen for each aneurysm, it will reduce significantly the flow induced in the cavity. The design of effective stents is therefore a key issue in this treatment technique, however there is no effective parameter to characterize the flow reduction capability of the stent because of the complexity in the flow reduction mechanism. Although several authors [4–12] have studied numerically and empirically the properties of stents on the induced flow in an aneurysm, no simple quantification of the flow reduction has been given, and no global characterization of the stent structure has been obtained to describe its effect. For example, the experimental and numerical results reported that the geometrical porosity and permeability of the stent has no significant correlation with its flow reduction property [13,14]. This means that it is difficult to predict the stent's effect in advance using these traditional parameters.

Here we propose to describe the flow reduction property of the stent using a stent positioning effect. The main result of the present work is to provide a meaningful stent parameter to characterize the flow reduction property and to reveal several other important stent parameters using this parameter. This result is valuable as it gives clear guidelines to stent manufacturers to aid effective design.

Our results follow from intensive numerical simulations in which we have analyzed the flow of blood with many different stents [14]. As we are looking for a generic effective parameter describing the quality of a stent, we consider the simplest possible two-dimensional situation, namely, the typical geometry presented in Fig. 1. We neglect several effects, such as the pulsatile flow of blood, its non-Newtonian properties, and the elasticity of the wall. It is indeed generally accepted that these aspects do not play a major role in how the stent structure affects the flow reduction [6,15–17]. Our numerical simulations are based on the lattice Boltzmann (LB) method [18,19], which represents a fluid as the discrete time dynamics of interacting the particle distribution function on a lattice. This approach has been successfully applied to various complex flow situations [18–21], including blood-flow simulations [22,23]. Our LB model is validated theoretically, experimentally, and numerically. Theoretically it is proved for the LB algorithm that the Navier-Stokes equations are recovered correctly for the small Mach number [24]. Compared with the results of the *in vitro* experiment in Ref. [8] and the numerical experiment using the traditional finite element method in Ref. [4], we can confirm that the results of our LB simulation in Ref. [14], where we

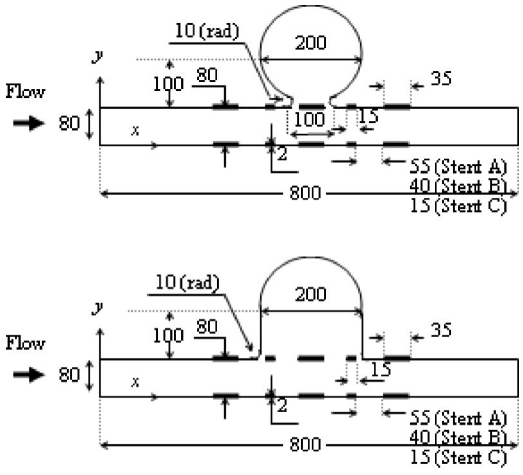

FIG. 1. A schematic view of an aneurysm on a parent vessel (unit: cell).

 ©2003 The American Physical Society

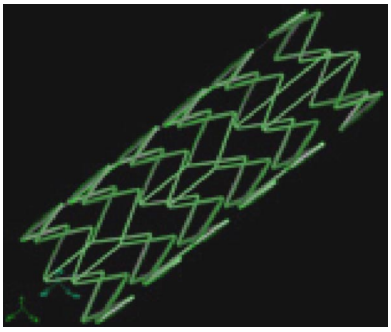

FIG. 2. (Color online) An example of a stent.

analyzed the flow pattern formation within the aneurysm in detail, show that our model can provide an effective simulation tool for the stented-blood-flow problem. Moreover compared with a traditional CFD solver, such as fluent, the LB approach is quite flexible and easy to adapt to various new conditions. For instance, in a forthcoming work, we shall consider explicitly the clotting effect, which we would like to describe as a deposition-aggregation process, similar to the LB sediment transport model of Refs. [25,26]. Also, we plan to include the wall elasticity in order to study aneurysm's growth and rupture, using the model described in Ref. [27].

The situation we consider is illustrated in Fig. 1. The size and parameters of the simulation are chosen so as to correspond to the range of experimental and clinical observations [3,8]. The stent is a tubular mesh which fits perfectly with the parent vessel width. In our two-dimensional simulation, the stent is represented by horizontal struts (see Fig. 1) with a thickness of two lattice cells. We use three types of stents A–C of different pore sizes and with relatively long periodic designs, which are suitable for measuring the two-dimensional positioning effect. The combination of the pore size and strut size is as follows: stent A (15-cell strut, 55-cell pore, 35-cell strut), stent B (15-cell strut, 40-cell pore, 35-cell strut), and stent C (15-cell strut, 15-cell pore, 35-cell strut), therefore the characteristic cyclic lengths of these stents are 160, 130, and 80 cells, respectively.

As for the aneurysm, we use two different cavities with a wide and a narrow neck in order to consider the influence of the neck size on the flow reduction. We use the following parameters based on the typical clinical observation of a saccular cerebral aneurysm. The aneurysm diameter is 10 mm and occupies 200 lattice cells in our simulation. The orifice diameter of the small-necked aneurysm is 5 mm and that of the large-necked aneurysm is 10 mm. The parent vessel is a straight tube, 4 mm wide (80 cells) and 40 mm long (800 cells).

In the parent vessel which we focus on, we can observe the following clinical flow parameters: the fluid density $\rho = 1.087 \times 10^3$ kg/m^3, fluid viscosity $\mu = 3.695 \times 10^{-3}$ Pa s, the average fluid velocity $u = 2.92 \times 10^{-1}$ m/s, the mean volume flow $Q = 2.2 \times 10^{-3}$ m^3/s, and systolic and diastolic pressure p of 1.9326×10^4 and 1.1996×10^4 Pa. We adjust the time and length scales between the numerical simulation and clinical data through the Reynolds number $\mathrm{Re} = \rho U l / \mu$, where U and l are the characteristic velocity and the characteristic length in the system. Here we use the average velocity $u = 2.92 \times 10^{-1}$ m/s in the parent vessel for the characteristic velocity U, and the diameter $d = 4.0 \times 10^{-3}$ m for the characteristic length l. Then we get the clinical Reynold number $\mathrm{Re} \simeq 344$ in the parent vessel. For the numerical study, we use the following flow parameters in order to get reasonable Reynolds number with numerical stability and efficiency [20]. Here we use the two-dimensional square lattice with nine velocities for the calculation, which is called the D2Q9 model [14,20]. The average density $\rho = 1.0$ and the kinematic viscosity of the lattice Boltzmann fluid $\nu = \mu/\rho = (2\tau - 1)/6 = 0.026$, where the relaxation time for the LB algorithm $\tau = 0.58$. The velocity at the center of the parent vessel $u = -(d^2/8\mu)\nabla p \simeq 0.1$, which is drawn by the pressure gradient $|\nabla p| = 4.17 \times 10^{-6}$ between the inlet and the outlet, is chosen as the characteristic velocity U. In our D2Q9 model the lattice Boltzmann sound speed $c_s = 1/\sqrt{3}$, therefore the Mach number $M = u/c_s \simeq 0.173$. The parent vessel diameter $d = 80$ is used for the characteristic length l. As a result we get the Reynolds number $\mathrm{Re} \simeq 307$ in the parent vessel.

The main flow obeys periodic boundary conditions along the x axis defined in Fig. 1, and is driven by a pressure gradient between the inlet and the outlet, which is imposed according to the method described in Ref. [28]. On the walls of the vessel and the aneurysm we use the so-called bounce-back rule [19,28–30], which ensures a nonslip boundary condition. On a stent element, the fluid particles also bounce back. The convergence criterion is attained by comparing simulation results from two successive time steps and the stop criterion is when this difference is less than 10^{-7}.

We show that we can characterize the flow reduction property of the stent in a quantitative way by introducing a measure of the flow reduction using the positioning effect. Here we define the stent positioning effect as the phenomenon caused by the variation of the strut position depending on the stent position at the aneurysm orifice. Numerically we can observe this effect by moving the stent from the initial position.

Figures 3 and 4 show that the variation of the stent strut position influences the effective porosity, which is defined as the metal-free area divided by the orifice area. The positioning error is defined as the distance from the initial position divided by the characteristic cyclic length of the stent. This effect is most remarkable in the small-necked aneurysm with the large-pore stent and in this case the variation of the flow reduction by the positioning effect is large. These figures show that the stent property depending on the aneurysm size can be described quantitatively by measuring the effective porosity using the stent positioning effect. Figures 5 and 6 show the variation in the velocity reduction depending on the positioning error. Here, the velocity reduction V_r is defined by computing a coefficient comparing the nonstented and the stented cases: $V_r = (U_{ns} - U_s)/U_{ns}$ where U_{ns} and U_s are the averages of the velocity $u = \sqrt{u_x^2(\mathbf{r}) + u_y^2(\mathbf{r})}$ over all lattice sites $\mathbf{r}(x,y)$ in the cavity, for nonstented and stented flows, respectively. The x axis and the y axis are defined in Fig. 1. The average velocity cannot reveal the mechanism of the localized stagnation within the aneurysm, which is thought

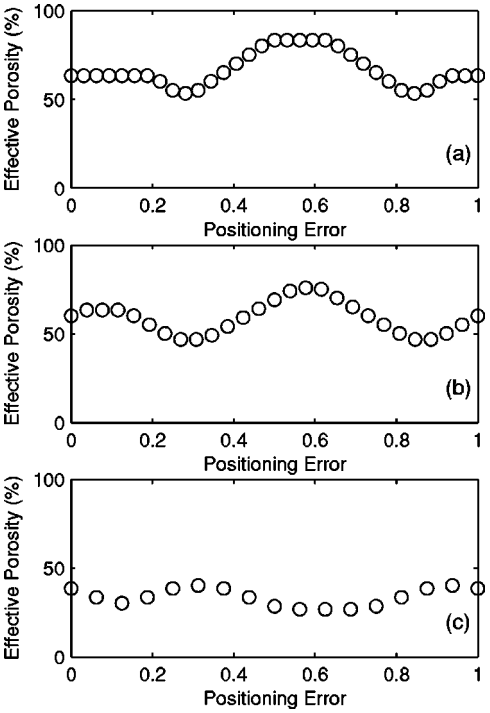

FIG. 3. Variation in the effective porosity at the small-necked aneurysm orifice when the stent is shifted along the cavity orifice successively by five cells: the positioning error is defined as the distance from the initial position divided by the characteristic cyclic length of the stent. (a) The case of stent *A*, (b) the case of stent *B*, and (c) the case of stent *C*. The variation in porosity is large at the small-necked aneurysm compared with the case at the large-necked aneurysm.

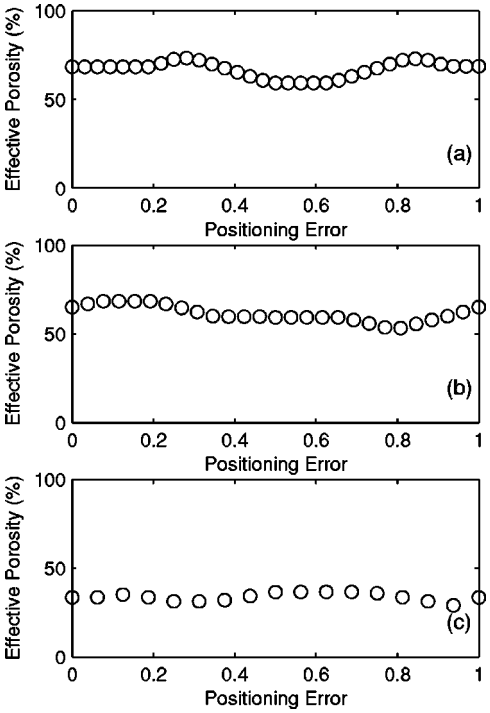

FIG. 4. Variation in the effective porosity at the large-necked aneurysm orifice when the stent is shifted along the cavity orifice successively by five cells. (a) The case of stent *A*, (b) the case of stent *B*, and (c) the case of stent *C*. The variation in porosity is not so large compared with the case of the small-necked aneurysm.

of as a cause of thrombotic occlusion, however, we focus on the total flow reduction property by stent implantation here. Figures 3–6 show the possibility that we can predict the velocity reduction effect by stent implantation in advance using the stent positioning effect. We can also characterize the velocity reduction property of the stent on each aneurysm using a Fourier series

$$V_r(\varepsilon) \simeq \frac{a_0}{2} + \sum_{n=1}^{\infty} a_n \cos 2n\pi\varepsilon + \sum_{n=1}^{\infty} b_n \sin 2n\pi\varepsilon, \quad (1)$$

where ε is the positioning error. The coefficients a_0, a_n, and b_n are stent-dependent parameters that provide a way to summarize the efficiency of a stent and, thus, give useful guidelines to design them.

Figures 5 and 6 also show the following features. Generally small-necked aneurysms have large velocity reduction error based on the stent position (see Fig. 5). This is remarkable in the large-pore stent (stent *A*). We think that this is due to the insufficient number of stent strut at the aneurysm orifice. This tendency is improved by using the small-pore stent (stent *B* or *C*). On the contrary, Fig. 6 shows that in the large-necked aneurysm the large-pore stent does not cause serious variations in flow reduction depending on the number of struts at the orifice, however this is sometimes the case for the small-pore stent. We think that this phenomenon is mainly caused by the strong orifice effect in the large-necked aneurysm. Compared with Fig. 7(c), Fig. 8(c) shows that the proportion maximum u_y of mean u at the aneurysm orifice is relatively large. This is due to a kind of orifice effect caused by the small pore in the stent and the relatively large velocity at the large-necked aneurysm orifice. These results show that the orifice effect cannot be neglected in determining the velocity reduction in large-necked aneurysms.

Flow reduction in an aneurysm by stent implantation is a complex phenomenon. Figures 3–6 show that there is no significant correlation between effective porosity and velocity reduction properties. These observations show that not only effective porosity but also strut distribution plays an important role in determination of the flow reduction effect. This is because it can be thought that the flow reduction mechanism is sensitive to the strut position due to the nonuniform velocity distribution at the aneurysm orifice, therefore the position of the strut at the aneurysm orifice is very important. Moreover the strut sometimes makes a narrow gap at the distal orifice. This also influences the orifice effect. These assumptions may explain the reason for the discontinuity in the variation in these figures. These phenomena, which are considered to be caused by the stent positioning effect or the orifice effect, have been observed experimentally [13]. We think that the stent positioning effect makes it difficult to analyze clinical observations, because it is difficult to know the exact stent position at the aneurysm orifice, therefore these numerical analyses will be helpful in understanding the clinical stent effect.

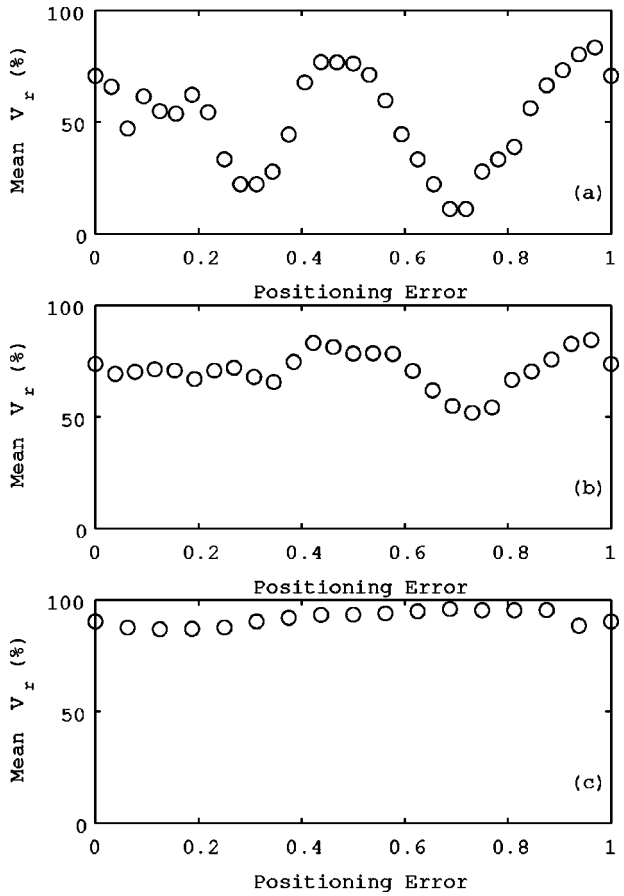

FIG. 5. Mean velocity reduction plots at the small-necked aneurysm orifice as a function of the positioning error. (a) The case of stent *A*, (b) the case of stent *B*, and (c) the case of stent *C*.

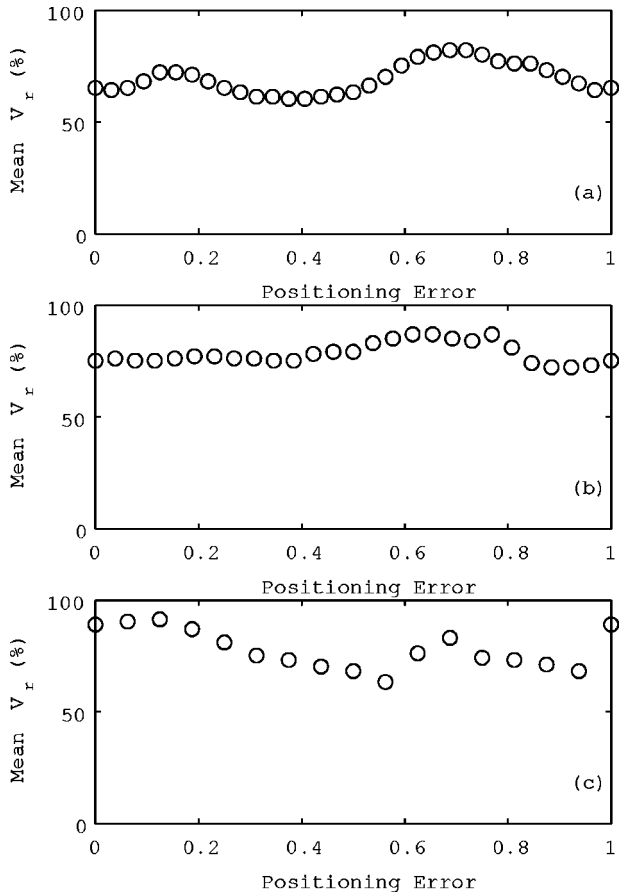

FIG. 6. Mean velocity reduction plots at the large-necked aneurysm orifice as a function of the positioning error. (a) The case of stent *A*, (b) the case of stent *B*, and (c) the case of stent *C*.

In conclusion, we have provided a useful guideline, the stent positioning measurement, in order to analyze the flow reduction effect in a cerebral artery with an aneurysm by stent implantation. The following four main analyses were obtained using this stent positioning measurement. First, the stent positioning effect cannot be neglected and therefore we can characterize the flow reduction property of a stent for each aneurysm by a Fourier series [Eq. (1)] utilizing this positioning effect. Second, a large-pore stent shows large fluctuation in the flow reduction for the small-necked aneurysm. We think that this is due to the small number of struts at the aneurysm orifice. This phenomenon depends mainly on the pore size (or effective porosity) of a stent. We guess that we can find the critical value of a combination of both the pore size and the aneurysm orifice size for characterizing these fluctuations. Third, a kind of orifice effect of the stent with small pores in the large-necked aneurysm disturbs the velocity reduction. This phenomenon depends mainly on the geometrical pore size, however, sometimes the strut position can cause another orifice effect because even a large-pore stent can make a narrow gap at the distal part of the aneurysm orifice. This implies that exact strut position at the aneurysm orifice plays an important role in flow reduction. Finally, the strut position (or strut distribution) at the aneurysm orifice must play another important role in the velocity reduction due to the nonuniform velocity distribution at the aneurysm orifice induced by the parent vessel flow. The effect of the flow reduction is sensitive to the strut distribution due to this nonuniformity. This may be one of the reasons for the existence of the discontinuity in the variation, which is observed in several figures.

We think that our analysis is effective in the three-dimensional case, too. As we mentioned before, the *in vitro* experiment in Ref. [8] shows a similar flow structure as our two-dimensional numerical simulation in Ref. [14]. In both cases, we can observe that the stent prevents the vortex in the aneurysm from being driven directly by the parent vessel flow. We provided the two-dimensional analysis of the mechanism of this flow pattern formation in detail in Ref. [14]. As for the stent design, the three-dimensional stent has more complex geometrical structure, however, the pore distribution and pore size should play the same important roles in this case, too. We think that the stent design parameters (such as the pore size, its distribution, the strut size, and its distribution) are very important factors in determining the flow structure. If the characteristic cyclic length of the stent is small (for example, a uniform fine-meshed stent), the stent positioning effect is not so remarkable as in our stent models used here. On the other hand, if the characteristic cyclic length of the stent is large (for example, a large-meshed stent), the flow reduction property is subject to the stent positioning effect and the strut distribution (or the pore distri-

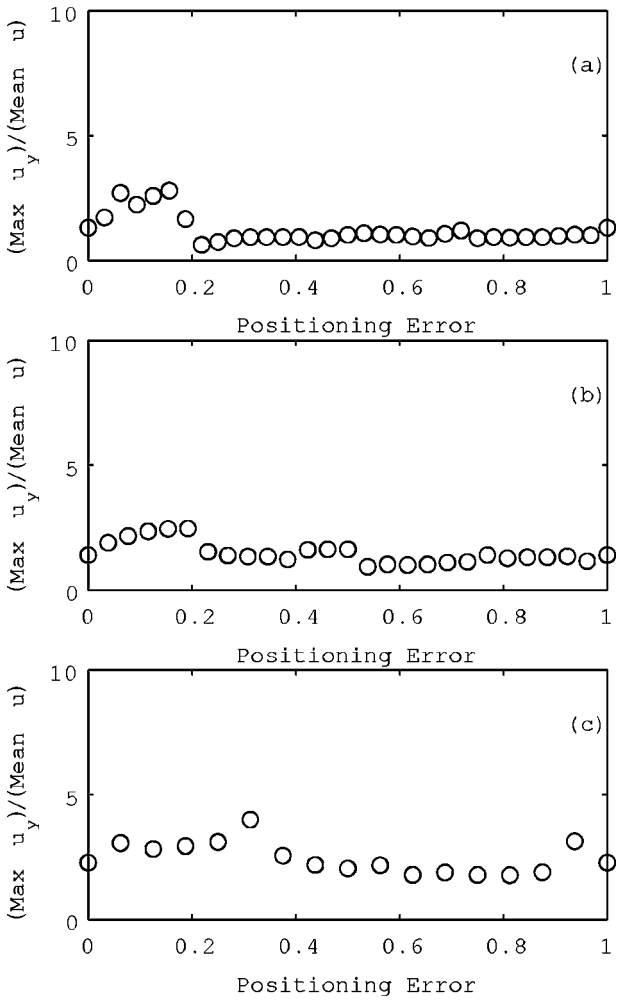

FIG. 7. The proportion maximum u_y of mean u plots at the small-necked aneurysm orifice with different positionings of the stent. (a) The case of stent *A*, (b) the case of stent *B*, and (c) the case of stent *C*.

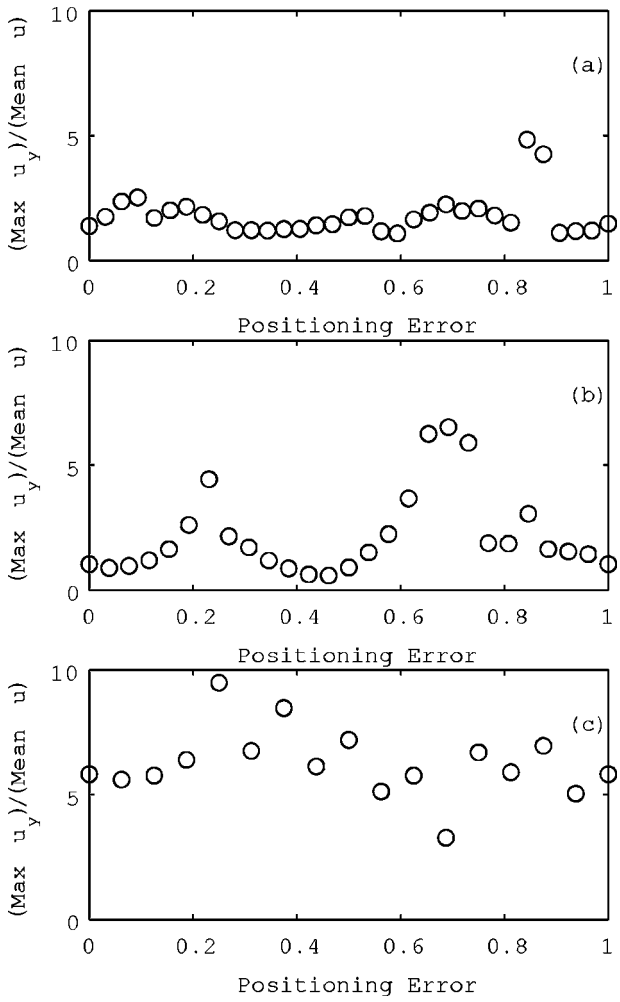

FIG. 8. The proportion maximum u_y of mean u plots at the large-necked aneurysm orifice with different positionings of the stent. (a) The case of stent *A*, (b) the case of stent *B*, and (c) the case of stent *C*.

bution) at the aneurysm orifice is also important for the flow pattern formation due to the nonuniform property of the velocity distribution at the aneurysm orifice. We expect that these design parameters can be classified using Eq. (1).

For future works, we think that we can propose some critical values of the combination of both stent parameters (such as the pore size or the strut size) and aneurysm parameters (such as the neck size or the dome size) on the flow reduction property by using the measurement of the positioning effect. Moreover the positioning effect will be useful to investigate the further flow structure for understanding the flow reduction mechanism by stent implantation. On a clinical note, it is difficult to confirm the stent positioning effect *in vivo*, because we cannot know the stent position at the aneurysm orifice in detail. However, we will be able to verify the existence of the stent positioning effect indirectly by observing the fact that the same stent shows different flow reduction properties in similar aneurysm situations. We think that this phenomenon, which is often observed in clinical operations, is caused by the large-pore stent, which is often used, because these stents are sensitive to the stent positioning effect. Our results offer an important framework to discuss the intricate properties of the stent.

We acknowledge the great help of Krisztina Baráth, Francis Cassot, Jonas Lätt, Alexandre Dupuis, and Christopher Pooley.

[1] D.A. Vorp, D.A. Steinman, and C.R. Ethier, IEEE Comput. Sci. Eng. **3**, 51 (2001).

[2] M.P. Marks, M.D. Dake, G.K. Steinberg, A.M. Norbash, and B. Lane, Radiology **191**, 441 (1994).

[3] A.K. Wakhloo, F. Schellhammer, J. de Vries, J. Haberstroh, and M. Schumacher, AJNR Am. J. Neuroradiol. **15**, 493 (1994).

[4] M. Aenis, A.P. Stancampiano, A.K. Wakhloo, and B.B. Lieber,

ASME J. Biomech. Eng. **119**, 206 (1997).
[5] G. Geremia, M. Haklin, and L. Brennecke, AJNR Am. J. Neuroradiol. **15**, 1223 (1994).
[6] B.B. Lieber, A.P. Stancampiano, and A.K. Wakhloo, Ann. Biomed. Eng. **25**, 460 (1997).
[7] T.M. Liou, W.C. Chang, and C.C. Liao, Exp. Fluids **23**, 317 (1997).
[8] S.C.M. Yu and J.B. Zhao, Med. Eng. Phys. **21**, 133 (1999).
[9] M. Hamuro, J.C. Palmaz, E.A. Sprague, C. Fuss, and J. Luo, J. Vasc. Interv Radiol. **12**, 607 (2001).
[10] S.G. Imbesi and C.W. Kerber, AJNR Am. J. Neuroradiol. **22**, 721 (2001).
[11] J.L. Berry, E. Manoach, C. Mekkaoui, P.H. Rolland, J.E. Moore, Jr., and A. Rachev, J. Vasc. Interv. Radiol. **13**, 97 (2002).
[12] C. Sadasivan, B.B. Lieber, M.J. Gounis, D.K. Lopes, and L.N. Hopkins, AJNR Am. J. Neuroradiol. **23**, 1214 (2002).
[13] K. Baráth, F. Cassot, J.H.D. Fasel, M. Ota, M. Hirabayashi, B. Chopard, and D.A. Rüfenacht, American Society of Neuroradiology 2003 Proceedings, p. 249 (unpublished).
[14] M. Hirabayashi, M. Ohta, D.A. Rüfenacht, and B. Chopard, in *Computational Science—ICCS 2003*, Proceedings Part I [Lect. Notes Comput. Sci. **2657**, 1044 (2003)].
[15] M. Löw, K. Perktold, and R. Rauning, Biorheology **30**, 287 (1993).
[16] K. Perktold, T. Kenner, D. Hilbert, B. Spork, and H. Florian, Basic Res. Cardiol. **83**, 24 (1988).
[17] K. Perktold, R. Peter, and M. Resch, Biorheology **26**, 1011 (1989).
[18] D.H. Rothman and S. Zaleski, *Lattice-Gas Cellular Automata* (Cambridge University Press, Cambridge, England, 1997).
[19] S. Chen and G.D. Doolen, Annu. Rev. Fluid Mech. **30**, 329 (1998).
[20] S. Succi, *The Lattice Boltzmann Equation for Fluid Dynamics and Beyond* (Oxford Science, Oxford, 2001).
[21] B. Chopard and M. Droz, *Cellular Automata Modeling of Physical Systems* (Cambridge University Press, Cambridge, 1998).
[22] H. Fang, Z. Wang, Z. Lin, and M. Liu, Phys. Rev. E **65**, 051925 (2002).
[23] A.M.M. Artoli, A.G. Hoekstra, and P.M.A. Sloot, in *Computational Science—ICCS 2002*, Proceedings Part I [Lect. Notes Comput. Sci. **2329**, 361 (2002)].
[24] H. Chen, S. Chen, and W.H. Matthaeus, Phys. Rev. A **45**, R5339 (1992).
[25] B. Chopard and A. Dupuis, Comput. Phys. Commun. **147**, 509 (2002).
[26] A. Dupuis and B. Chopard, J. Comput. Phys. **178**, 161 (2002).
[27] B. Chopard and S. Marconi, Fluid. J. Stat. Phys. **107**, 23 (2002).
[28] A. Dupuis, Doctoral thesis, University of Geneva, 2002, http://cui.unige.ch/spc/PhDs/aDupuisPhD/phd.html
[29] D. Ziegler, J. Stat. Phys. **71**, 1171 (1993).
[30] P.A. Skordos, Phys. Rev. E **48**, 4823 (1993).